

pubs.acs.org/JPCA Article

Linear Scaling Calculations of Excitation Energies with Active-Space Particle—Particle Random-Phase Approximation

Published as part of The Journal of Physical Chemistry A virtual special issue "Krishnan Raghavachari Festschrift".

Jiachen Li, Jincheng Yu, Zehua Chen, and Weitao Yang*



Cite This: J. Phys. Chem. A 2023, 127, 7811-7822



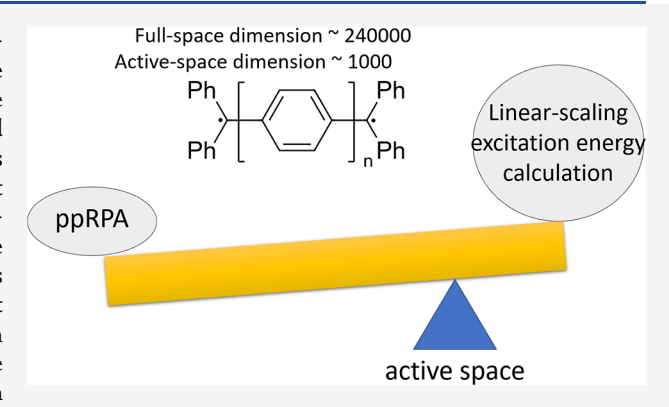
ACCESS I

III Metrics & More

Article Recommendations

si Supporting Information

ABSTRACT: We developed an efficient active-space particle—particle random-phase approximation (ppRPA) approach to calculate accurate charge-neutral excitation energies of molecular systems. The active-space ppRPA approach constrains both indexes in particle and hole pairs in the ppRPA matrix, which only selects frontier orbitals with dominant contributions to low-lying excitation energies. It employs the truncation in both orbital indexes in the particle—particle and the hole—hole spaces. The resulting matrix, whose eigenvalues are excitation energies, has a dimension that is independent of the size of the systems. The computational effort for the excitation energy calculation, therefore, scales linearly with system size and is negligible compared with the ground-state calculation of the (N-2)-electron system, where N is the electron



number of the molecule. With the active space consisting of 30 occupied and 30 virtual orbitals, the active-space ppRPA approach predicts the excitation energies of valence, charge-transfer, Rydberg, double, and diradical excitations with the mean absolute errors (MAEs) smaller than 0.03 eV compared with the full-space ppRPA results. As a side product, we also applied the active-space ppRPA approach in the renormalized singles (RS) T-matrix approach. Combining the non-interacting pair approximation that approximates the contribution to the self-energy outside the active space, the active-space $G_{\rm RS}T_{\rm RS}$ @PBE approach predicts accurate absolute and relative core-level binding energies with the MAEs around 1.58 and 0.3 eV, respectively. The developed linear scaling calculation of excitation energies is promising for applications to large and complex systems.

■ INTRODUCTION

The accurate description for charge-neutral (optical) excitations is important for understanding optical spectroscopies. In past decades, many theoretical approaches have been developed to compute excitation energies. Time-dependent density functional theory 1-3 (TDDFT) ranks among the most used approach for finite systems because of the good compromise between the accuracy and the computational cost. TDDFT with commonly used density functional approximations (DFAs) has been widely applied to predict the excitation energies of different systems including molecules, liquids, and solids.⁴⁻⁶ However, it is well known that TDDFT with conventional DFAs provides an incorrect long-range behavior. 7,8 Consequently, TDDFT fails to describe Rydberg and charge-transfer (CT) excitations.^{7,8} Efforts including using range-separated functionals 9-12 and tuning the amount of the Hartree-Fock (HF) exchange in DFAs 13-15 have been made to address this issue. In addition, the accuracy of TDDFT largely depends on the exchange-correlation (XC) kernel.⁶ Different from TDDFT, the Bethe-Salpeter equation^{16–18} (BSE) formalism has also gained increasing attention. BSE commonly takes the quasiparticle (QP) energies from the GW approximation^{19–22} to calculate the excitation energies, which is the BSE/GW approach. Because of the correct description for the long-range behavior and the dynamical screening interaction in real systems, BSE/GW is shown to predict accurate excitation energies for various kinds of systems.^{23–27} However, the accuracy of the BSE/GW formalism strongly depends on the level of the self-consistency in the preceding GW calculation and is affected by the approximation that ignores the frequency dependence and the derivative of the screened interaction to Green's function in the BSE kernel. BSE combined with the one-shot G_0W_0

Received: April 29, 2023
Revised: August 23, 2023
Published: September 11, 2023





method has the undesired starting point dependence²⁷⁻²⁹ similar to TDDFT. BSE combined with the eigenvalue-selfconsistent GW (evGW) method shows great improvements over BSE/ G_0W_0 but brings extra computational costs. 27,30,31 Efforts including combining BSE with the renormalized singles Green's function²⁷ and using the optimal starting point²⁴ have been made to improve the accuracy and reduce the computational cost. Recently, approaches combining BSE with generalized Kohn-Sham (KS) methods, including localized orbital scaling correction³² (LOSC) and Koopmans-compliant functionals,³³ have been developed to bypass the computationally demanding GW calculation. BSE combined with the T-matrix approximation has also been reported.³⁴ In addition to the computationally affordable BSE and TDDFT formalisms, wave function approaches with high accuracy are also used to predict excitation energies, including complete active space second-order perturbation theory³⁸ (CASPT2) and coupled cluster methods^{36,37} (CC3, CCSDT). However, due to the demanding computational cost, wave function approaches are usually used for benchmarks. 38-40

The particle-particle random-phase approximation (ppRPA), originally developed to describe the nuclear manybody correlation, 41-43 has been applied to describe the ground-state and excited-state properties of molecular systems. 44,45 ppRPA can be derived from different approaches, including the adiabatic connection 44,45 as a parallel to the traditional adiabatic connection using the particle—hole density fluctuations, ^{46,47} TDDFT with the pairing field, ⁴⁸ and the equation of motion. ^{49,50} As a counterpart to the commonly used particle-hole random-phase approximation^{51,52} (phRPA), ppRPA conveys information in the particle-particle and hole-hole channels, which leads to the two-electron addition and two-electron removal energies. Thus, the excitation energy of the N-electron system can be obtained by the difference between the two-electron addition energies of the (N-2)-electron system. ⁴³ The same set of equations were also applied for describing the excited states of the N-electron molecule using the hole-hole excitations of the corresponding (N + 2)-electron system.^{53,54} ppRPA has been shown to predict accurate excitation energies of different characteristics including the singlet-triplet (S-T) gaps of diradicals, double excitations, CT excitations, Rydberg excitations, and valence excitations. It also describes conical intersections and oscillator strengths well. 43,55 The success of ppRPA for predicting the excitation energies of molecular systems can be attributed to several reasons. First, ppRPA can be viewed as a Fock-space embedding approach that treats two frontier electrons in a subspace configuration interaction fashion with a seamless combination of density functional theory 56,57 (DFT) for the remaining (N-2) electrons. 58,59 Thus, ppRPA provides an accurate description of the static correlation of the two nonbonding electrons in the diradical systems. 58,60 Second, ppRPA contains the information in the particle-particle channel and is naturally capable of describing double excitations, 43 which cannot be captured by TDDFT or BSE with the static approximation. 61,62 Third, because the ppRPA kernel provides the correct long-range asymptotic behavior, ppRPA can accurately predict CT and Rydberg excitation energies. 43,63 Finally, the ppRPA kernel is independent of the DFA reference; thus, the starting point dependence of ppRPA is smaller than TDDFT. 63,64 Recently, ppRPA with the Tamm-Dancoff approximation (TDA) has been applied in the multireference DFT approach to provide accurate dissociation

energies and excitation energies.^{65,66} In addition to the calculation of the excitation energy, the ppRPA eigenvalues and eigenvectors are also used in the T-matrix approximation to calculate QP energies.^{67,68}

However, it is challenging to apply ppRPA to compute the excitation energies of large systems due to its relatively high computational cost. In ppRPA, the two-electron integrals of four virtual orbitals are needed. 44,64 Because the number of virtual orbitals $N_{\rm vir}$ is generally much larger than the number of occupied orbitals $N_{\rm occ}$, the dimension of ppRPA is much larger than the dimension of TDDFT or BSE. ⁵⁹ Although the formal scaling of solving the ppRPA equation can be reduced to $O(N^4)$ by using the Davidson algorithm^{64,69} (N is the size of the system), the size of the ppRPA matrix has a large prefactor compared with those of TDDFT and BSE. The active-space ppRPA approach has recently been developed to reduce the computational cost.⁵⁹ In the active-space ppRPA approach, the ppRPA matrix is constructed and diagonalized in an active space, which consists of a predetermined number of frontier orbitals near the highest occupied molecular orbital (HOMO) and the lowest unoccupied molecular orbital (LUMO).⁵⁹ In principle, the natural orbitals from diagonalizing the density matrix of a correlated method can be used to construct the active space and further reduce the computational cost. As shown in ref 59, the convergence of excitation energies obtained from the active-space ppRPA approach toward the full-space ppRPA results is rapid with respect to the size of the active space. The active-space ppRPA approach is shown to efficiently compute the excitation energies for different systems with only a modest number of active orbitals. However, a large amount of high-lying virtual orbitals are included in the original active-space ppRPA approach. These high-lying virtual orbitals have small contributions to the desired low-lying excitations, which lead to unnecessary computational burden and limit the application for larger systems.

In this work, we introduce a new active-space ppRPA approach that improves the efficiency and further reduces the computational cost. The new active-space ppRPA approach constrains both indexes in particle and hole pairs, which selects frontier orbitals by the summation of orbital energies and is shown to provide significantly better efficiency than the original active-space ppRPA approach.⁵⁹ We also extend the active-space ppRPA approach to the T-matrix approximation^{67,68} for core-level QP energy calculations. In the activespace T-matrix approach, the self-energy in the active space is formulated with eigenvalues and eigenvectors obtained from the preceding active-space ppRPA approach. To capture the contribution to the self-energy outside the active space, we develop the non-interacting pair (NIP) approximation that only uses KS orbitals and orbital energies to approximate the ppRPA eigenvalues and eigenvectors. We show that the activespace T-matrix approach combined with the recently developed RS Green's function, ^{68,70-72} which is shown to be a good starting point for Green's function formalism, is capable of predicting accurate core-level binding energies (CLBEs).

METHODS

Excitation Energies from ppRPA. We first review the ppRPA formalism. Similar to the phRPA that is formulated in terms of density fluctuation, ppRPA is formulated with the fluctuation of the pairing matrix 42,44,45,49

$$\kappa(x_1, x_2) = \langle \Psi_0^N | \hat{\psi}(x_2) \hat{\psi}(x_1) | \Psi_0^N \rangle \tag{1}$$

where $x=(r,\sigma)$ is the space—spin combined variable, Ψ^N_0 is the N-electron ground state, and $\hat{\psi}^\dagger$ and $\hat{\psi}$ are the second quantization creation and annihilation operator, respectively. While the paring matrix is zero for electronic ground states, the response of the pairing matrix $\delta \kappa(x_1, x_2)$ is non-zero when the system is perturbed by an external pairing field. In the frequency space, the time-ordered pairing matrix fluctuation, the linear response function, has poles at two-electron addition and removal energies 42,44,45,49

$$K(\omega)_{pqrs} = \sum_{m} \frac{\langle \Psi_{0}^{N} | \hat{a}_{p} \hat{a}_{q} | \Psi_{0}^{N+2} \rangle \langle \Psi_{0}^{N+2} | \hat{a}_{s}^{\dagger} \hat{a}_{r}^{\dagger} | \Psi_{0}^{N} \rangle}{\omega - \Omega_{m}^{N+2} + i\eta}$$

$$- \sum_{m} \frac{\langle \Psi_{0}^{N} | \hat{a}_{s}^{\dagger} \hat{a}_{r}^{\dagger} | \Psi_{0}^{N-2} \rangle \langle \Psi_{0}^{N-2} | \hat{a}_{p} \hat{a}_{q} | \Psi_{0}^{N} \rangle}{\omega - \Omega_{m}^{N-2} - i\eta}$$

$$(2)$$

where \hat{a}_p^{\dagger} and \hat{a}_p are the second quantization creation and annihilation operator for the orbital p, respectively, $\Omega^{N\pm 2}$ is the two-electron addition/removal energy, and η is the positive infinitesimal number. We use i, j, k, and l for occupied orbitals; a, b, c, and d for virtual orbitals; p, q, r, and s for general orbitals; and m for the index of the two-electron addition/removal energy. To obtain the pairing matrix fluctuation K of the interacting system, ppRPA approximates K in terms of the non-interacting K_0 by the Dyson equation $\frac{44,45}{1}$

$$K = K^0 + K^0 V K \tag{3}$$

where the antisymmetrized interaction $V_{pqrs} = \langle pq || rs \rangle = \langle pq || rs \rangle - \langle pq || sr \rangle$ is defined as

$$\langle pq || rs \rangle = \langle pq | rs \rangle - \langle pq | sr \rangle$$
 (4)

$$= \int dx_1 dx_2 \frac{\phi_p^*(x_1)\phi_q^*(x_2)(1-\hat{P}_{12})\phi_r(x_1)\phi_s(x_2)}{|r_1-r_2|}$$
(5)

Direct ppRPA can be obtained if the exchange term is neglected in $V^{.73}$

Equation 3 can be substituted into a generalized eigenvalue equation, which describes the two-electron addition/removal excitations 43,44,64

$$\begin{bmatrix} A & B \\ B^T & C \end{bmatrix} \begin{bmatrix} X \\ Y \end{bmatrix} = \Omega^{N\pm 2} \begin{bmatrix} I & 0 \\ 0 & -I \end{bmatrix} \begin{bmatrix} X \\ Y \end{bmatrix}$$
(6)

with

$$A_{ab,cd} = \delta_{ac}\delta_{bd}(\epsilon_a + \epsilon_b) + \langle ab||cd\rangle \tag{7}$$

$$B_{ab,kl} = \langle ab || kl \rangle \tag{8}$$

$$C_{ij,kl} = -\delta_{ik}\delta_{jl}(\epsilon_i + \epsilon_j) + \langle ij||kl\rangle \tag{9}$$

where a < b, c < d, i < j, k < l, and $\Omega^{N\pm 2}$ are the two-electron addition/removal energies. To obtain the charge-neutral excitations of the N-electron system, first the self-consistent field (SCF) calculation of the corresponding (N-2)-electron system at the same geometry is performed, and then the orbital energies and orbitals are used in the working equation of ppRPA (eq 6) for two-electron addition energies. The excitation energy can be obtained from the difference between the lowest and a higher two-electron addition energy. 74

Active-Space ppRPA Approach for Optical Excitation Energies. To reduce the computational cost, the active-space ppRPA approach has recently been developed. The motivation is to approximate the resonance modes by choosing a set of frontier orbitals in an active space⁵⁹

$$\begin{split} \delta\kappa(x_1,\,x_2,\,\Omega_m^{N\pm 2}) &\approx \, \sum_{A < b} X_{Ab}^{N\pm 2,m} \psi_A(x_1) \psi_b(x_2) \\ &+ \, \sum_{i < J} Y_{iJ}^{N\pm 2,m} \psi_i(x_1) \psi_j(x_2) \end{split} \tag{10}$$

where we use *A*, *B* for active virtual orbitals and *I*, *J* for active occupied orbitals. In eq 10, only one index in particle and hole pairs is constrained. So, the dimension of the active space introduced in ref 59 is

$$\frac{1}{2}(N_{\text{vir,act}} + 1)N_{\text{vir,act}} + N_{\text{vir,act}}(N_{\text{vir}} - N_{\text{vir,act}})
+ \frac{1}{2}(N_{\text{occ,act}} + 1)N_{\text{occ,act}} + N_{\text{occ,act}}(N_{\text{occ}} - N_{\text{occ,act}})$$
(11)

which depends on the size of the active space and linearly on the size of the full system. As shown in ref 59, this active-space ppRPA approach has small errors of 0.05 eV for excitation energies toward the full-space ppRPA results with the scaling of $O(N^4)$. However, this active-space ppRPA approach can still have challenges for calculating large systems because it only constrains one index in particle and hole pairs and includes high-lying virtual orbitals that have small contributions to the low-lying excitations.

In this work, we introduce a new active-space ppRPA approach to further reduce the computational cost. The new active-space ppRPA approach constrains both indexes in particle pairs and hole pairs, which means

$$\delta\kappa(x_{1}, x_{2}, \Omega_{m}^{N\pm2}) \approx \sum_{A < B < N_{\text{vir,act}}} X_{AB}^{N\pm2,m} \psi_{A}(x_{1}) \psi_{B}(x_{2}) + \sum_{I < J < N_{\text{occ,act}}} Y_{IJ}^{N\pm2,m} \psi_{I}(x_{1}) \psi_{J}(x_{2})$$
(12)

Therefore, the active space only includes low-lying virtual orbitals that have dominant contributions to the calculations of low-excitation energies. High-lying orbitals can be excluded from the active space without losing the accuracy. In ref 59, the active space only constrains one index in X and Y, which includes a large amount of high-lying excitations and leads to the $O(N^3)$ scaling. The dimension of the new active space is

$$\frac{1}{2}(N_{\text{vir,act}} + 1)N_{\text{vir,act}} + \frac{1}{2}(N_{\text{occ,act}} + 1)N_{\text{occ,act}}$$
(13)

which only depends on the size of the active space, not on the system size. Therefore, the scaling for the active-space ppRPA approach is O(N) when a constant number of orbitals are included in the active space for the construction of the three-center resolution of identity (RI) or the density-fitting matrix in the ground-state calculation.

Active-Space T-Matrix Approach for Core-Level Quasiparticle Energies. The active-space ppRPA approach can be directly applied in the T-matrix approximation. The T-matrix self-energy is the counterpart of the *GW* self-energy in the particle–particle channel, which is the summation of all ladder diagrams and is formulated with ppRPA. 67,68 In the

frequency space, the correlation part of the self-energy in the T-matrix approximation is ^{67,68}

$$\Sigma_{pq}^{c}(\omega) = \sum_{m} \sum_{i} \frac{\langle pi|\chi_{m}^{N+2}\rangle\langle qi|\chi_{m}^{N+2}\rangle}{\omega + \epsilon_{i} - \Omega_{m}^{N+2} + i\eta} + \sum_{m} \sum_{a} \frac{\langle pa|\chi_{m}^{N-2}\rangle\langle qa|\chi_{m}^{N-2}\rangle}{\omega + \epsilon_{a} - \Omega_{m}^{N-2} - i\eta}$$
(14)

In eq 14, the transition density is

$$\langle pi|\chi_m^{N+2}\rangle = \sum_{c < d} \langle pi||cd\rangle X_{cd}^{N+2,m} + \sum_{k < l} \langle pi||kl\rangle Y_{kl}^{N+2,m}$$
(15)

$$\langle pa|\chi_m^{N-2}\rangle = \sum_{c < d} \langle pa||cd\rangle X_{cd}^{N-2,m} + \sum_{k < l} \langle pa||kl\rangle Y_{kl}^{N-2,m}$$

$$\tag{16}$$

where $X_m^{N\pm 2}$, $Y_m^{N\pm 2}$, and $\Omega_m^{N\pm 2}$ are two-electron addition/removal eigenvectors and eigenvalues from ppRPA, respectively. Since all excitations in ppRPA are needed to formulate the T-matrix self-energy, the scaling for the ppRPA step is of $O(N^6)$. The scaling of evaluating the T-matrix self-energy in eq 14 is also of $O(N^6)$.

In our active-space T-matrix approach, the self-energy is divided into two parts: the contribution from the active space and the contribution outside the active space. For the contribution from the active space, the correlation part of the self-energy is formulated with the eigenvalues and eigenvectors obtained from the active-space ppRPA approach

$$\Sigma_{pq}^{c,act}(\omega) = \sum_{m}^{\text{act}} \frac{\langle pi|\chi_{m}^{N+2}\rangle\langle qi|\chi_{m}^{N+2}\rangle}{\omega + \epsilon_{i} - \Omega_{m}^{N+2} - i\eta} + \sum_{m}^{\text{act}} \frac{\sum_{i}^{N_{\text{vir,act}}} \frac{\langle pi|\chi_{m}^{N+2}\rangle\langle qi|\chi_{m}^{N-2}\rangle}{\omega + \epsilon_{a} - \Omega_{m}^{N-2} + i\eta}$$

$$(17)$$

where "act" means the contribution from the active space. The scaling of solving the ppRPA equation and evaluating the self-energy within the active space is of $O(N^6)$, which is the same as the full-space T-matrix approach. However, because the indexes are constrained in the active space, a small prefactor can be obtained.

To include the contribution outside the active space, we introduce the NIP approximation. In the NIP approximation, for the excitation m corresponding to the (p, q) pair, the two-electron addition/removal energy is simply approximated by the KS orbital energies

$$\Omega_{pq}^{N\pm 2} = \pm (\epsilon_p + \epsilon_q) \tag{18}$$

and the corresponding eigenvector is

$$X = I \text{ and } Y = I \tag{19}$$

Therefore, the correlation part of the self-energy from the NIP approximation is

$$\Sigma_{pq}^{c,\text{out}}(\omega) = \sum_{jk}^{\text{out}} \sum_{i} \frac{\langle pi || jk \rangle \langle qi || jk \rangle}{\omega + \epsilon_{i} - (\epsilon_{j} + \epsilon_{k}) - i\eta} + \sum_{bc}^{\text{out}} \sum_{a} \frac{\langle pa || bc \rangle \langle qa || bc \rangle}{\omega + \epsilon_{a} - (\epsilon_{b} + \epsilon_{c}) + i\eta}$$
(20)

where "out" in the summations means indexes outside the active space. In the NIP approximation, the ppRPA eigenvectors outside the active space act as an identity matrix, which approximates the transition density by the dominant two-electron integrals. As shown in Table 7, treating ppRPA exactly in the active space and approximately by the NIP approximation outside the active space provides similar results to the full-space results for the CORE65 test set. The scaling of evaluating the self-energy with the NIP approximation in eq 20 is of $O(N^5)$.

■ COMPUTATIONAL DETAILS

We implemented the active-space ppRPA approach and the active-space T-matrix approach in the QM4D quantum chemistry package. For the active-space ppRPA approach, we tested five different types of excitations: the S-T gaps of diradical systems, the CT excitation energies of the Stein CT test set, the double-excitation energies of small atomic and molecular systems, the Rydberg excitation energies of atomic systems, the valence excitation energies of the Thiel test set, the Tozer test set. For S-T gaps of diradical systems, the aug-cc-pVDZ basis set the S1,82 was used. Geometries and reference values were taken from ref 60. For the adiabatic S-T gaps, corrections obtained from the SCF calculations of the N-electron system are added to vertical S-T gaps

$$E_{g_a} = E_{g_{v,Sgeo}} + (E_{T,Sgeo} - E_{T,Tgeo})$$
 (21)

where $E_{\rm g_a}$ is the adiabatic S–T gap, $E_{\rm g_{v,\rm Sgeo}}$ is the vertical S–T gap, $E_{T,Sgeo}$ is the triplet energy of the N-electron system of the singlet geometry, and $E_{T,Tgeo}$ is the triplet energy of the Nelectron system of the triplet geometry. For the Stein CT test set, 76 the cc-pVDZ basis set 81 was used. Geometries and experimental values in the gas phase were taken from ref 76. For double excitations, the even-tempered basis set defined in ref 43 was used for Be and Li, the cc-pVQZ basis set⁸¹ was used for BH, the aug-cc-pVDZ basis set 81,82 was used for C, and the cc-pVDZ basis set 81 was used for H in polyenes. Geometries were optimized at the MP2/6-31G* level with the GAUSSIAN16 A.03 software.83 Reference values were taken from ref 43. For Rydberg excitations, the aug-cc-pVQZ basis set was used. 81,82 Reference values were taken from ref 77. For the Thiel test set^{78,79} and the Tozer test set,⁸⁰ the aug-cc-pVDZ basis set^{81,82} was used. Geometries and reference values were taken from refs 78-80. For the hydrocarbon diradical calculations, the cc-pVDZ basis set⁸¹ was used. The closedshell singlet geometries were taken from ref 84. Reference values were taken from refs 85 and 86. For the active-space Tmatrix approach, the CLBEs in the CORE65 test set⁸⁷ were calculated. The def2-TZVP basis set⁸⁸ was used. Geometries and reference values were taken from ref 87. QM4D uses Cartesian basis sets and uses the RI technique 89-91 to compute two-electron integrals. All basis sets and the corresponding fitting basis sets ^{92,93} were taken from the Basis Set Exchange. ^{94–96}

RESULTS

Comparison between Different Active-Space ppRPA Approaches. We first compare the active-space ppRPA approach developed in this work and in ref 59. The excitation energies of the ${}^{3}B_{2}$ of cyclopropene and the first singlet state of o-xylene obtained by different active-space ppRPA approaches

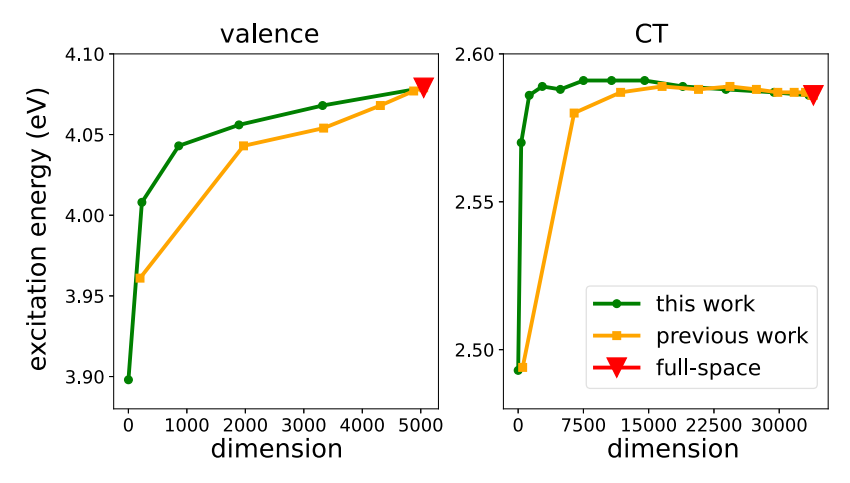


Figure 1. Comparisons of excitation energies obtained from the active-space ppRPA approach in this work and in ref 59 with respect to the dimension of the ppRPA matrix. The active spaces include all occupied orbitals and different numbers of virtual orbitals. The dimensions of active spaces are calculated from eqs 11 and 13. Left: ${}^{3}B_{2}$ state of cyclopropene. The full-space dimension is 5050. Right: first singlet state of o-xylene. The full-space dimension is 33,930. The aug-cc-pVDZ basis set was used for cyclopropene; the cc-pVDZ basis set was used for o-xylene.

Table 1. Adiabatic Singlet-Triplet Gaps and MAEs of Diradicals Obtained from the Full-Space and Active-Space ppRPA Approaches Based on HF, PBE, and B3LYP^a

11	•	•									
				HF			PBE			B3LYP	
	state	ref	full	(30,30)	(20,20)	full	(30,30)	(20,20)	full	(30,30)	(20,20)
°CH ₂ CH ₂ CH ₂ °		1.8	2.4	2.7	3.1	5.4	5.9	5.9	4.4	4.8	4.8
•CH ₂ (CH ₂) ₄ CH ₂ •	$^{1}A_{1}$	0.0	0.0	0.0	0.0	0.1	0.1	0.1	0.1	0.1	0.1
	$^{1}B_{1}$	160.8	79.9	79.8	79.8	159.2	159.4	159.5	147.4	147.5	147.6
	$2^{1}A_{1}$	163.1	80.6	80.5	80.5	162.0	162.0	162.5	149.0	149.1	149.5
${}^{\bullet}CH_2(CH_2)_4C(CH_3)H^{\bullet}$	$^{1}A_{1}$	-0.2	-0.3	-0.3	-0.3	0.4	0.4	0.4	0.1	0.1	0.1
	$2^{1}A_{1}$	131.1	66.1	65.6	65.6	139.8	139.7	140.2	129.1	129.0	129.2
	3^1A_1	144.3	78.3	77.7	78.0	152.4	152.4	152.5	142.1	142.1	142.0
cyclobutadiene		7.2	7.0	7.8	6.5	6.4	6.9	5.3	6.5	7.1	5.6
NH		35.9	30.9	30.9	31.0	40.5	40.5	40.8	38.5	38.5	38.7
OH+		50.5	45.5	45.5	45.7	54.2	54.2	54.5	52.2	52.3	52.6
NF		34.3	28.5	29.4	29.0	28.3	29.1	28.7	28.6	29.5	29.1
O_2		22.6	23.1	23.3	24.7	23.5	23.7	24.9	23.6	23.8	25.0
CH ₂	$^{1}A_{1}$	9.7	-1.9	-1.3	-0.7	6.3	7.2	8.0	4.2	5.1	5.8
	$^{1}B_{1}$	32.5	27.4	27.7	27.1	34.6	35.1	34.8	33.2	33.6	33.3
	$2^{1}A_{1}$	58.3	49.3	49.8	48.8	58.8	59.6	59.3	56.9	57.7	57.3
NH ₂ ⁺	$^{1}A_{1}$	28.9	12.8	14.7	15.3	25.6	27.8	28.2	23.0	25.2	25.6
	$^{1}B_{1}$	43.0	36.4	36.9	38.0	43.7	44.3	45.2	42.0	42.6	43.6
	$2^{1}A_{1}$	76.5	62.1	65.5	66.8	72.3	76.4	77.9	70.0	74.0	75.5
SiH_2	${}^{1}A_{1}$	-20.6	-25.0	-24.5	-25.0	-28.4	-27.7	-26.9	-28.8	-28.2	-27.3
	$^{1}B_{1}$	24.1	24.0	24.0	25.4	26.4	26.5	27.5	26.2	26.3	27.4
	2^1A_1	57.0	51.3	51.5	54.3	52.2	52.5	54.6	53.5	53.8	55.9
PH_2^+	$^{1}A_{1}$	-18.3	-25.3	-24.7	-23.8	-23.6	-23.0	-22.3	-24.7	-24.0	-23.3
	$^{1}B_{1}$	27.6	28.8	29.1	30.3	30.1	30.3	31.0	30.0	30.2	31.0
	$2^{1}A_{1}$	65.6	60.1	60.7	62.2	59.4	59.7	62.5	60.6	60.9	63.9
MAE			36.9	37.2	37.2	3.1	3.0	3.2	4.4	4.4	4.5

"Full stands for the full space. (20,20)/(30,30) means 20/30 occupied and virtual frontier orbitals are included in the active space. Geometries and reference values were taken from ref 60. The aug-cc-pVDZ basis set was used. All values in kcal/mol.

are shown in Figure 1. For simplicity, the active spaces include all occupied orbitals and the varying number of virtual orbitals. As shown in the left of Figure 1, the active-space ppRPA approach in this work has better convergence behavior than that in ref 59. The reason is that the active-space ppRPA approach in ref 59 constrains only one index in particle pairs, which includes high-lying particle pairs with small contributions to the low-lying excitation energies. As shown on the

right-hand side of Figure 1, for the CT excitation energy, both active-space ppRPA approaches with a small number of virtual orbitals in the active space produce errors smaller than 0.05 eV compared with the full-space results. For the CT excitations, the excitation energy converges rapidly with respect to the dimension of the active space. With the further increase of the active space, the excitation energy slightly decreases to the full-space result because of the stabilization from the high-lying

Table 2. CT Excitation Energies and MAEs in the Stein CT Test Set Obtained from the Full-Space and Active-Space ppRPA Approaches Based on HF, PBE, and B3LYP^a

		HF				PBE		B3LYP		
	ref	full	(30,30)	(20,20)	full	(30,30)	(20,20)	full	(30,30)	(20,20)
anthracene	2.05	1.95	1.92	1.91	1.25	1.21	1.20	1.36	1.32	1.32
9-cyano	2.33	1.99	1.93	1.92	1.35	1.34	1.31	1.49	1.45	1.42
9-chloro	2.06	1.91	1.87	1.86	1.19	1.16	1.13	1.31	1.26	1.23
9-carbomethoxy	2.16	1.92	1.87	1.86	1.18	1.13	1.10	1.30	1.25	1.22
9-methyl	1.87	1.70	1.67	1.66	1.05	1.02	0.99	1.15	1.12	1.10
9,10-dimethyl	1.76	1.78	1.77	1.76	1.07	1.05	1.04	1.19	1.18	1.16
9-formyl	2.22	2.08	2.04	2.03	1.43	1.40	1.37	1.50	1.46	1.44
9-formyl, 10-chloro	2.28	2.13	2.09	2.07	1.41	1.38	1.35	1.51	1.47	1.44
benzene	3.91	2.58	2.38	2.36	3.18	3.23	3.23	3.46	3.50	3.55
toluene	3.68	2.30	2.17	2.15	2.77	2.81	2.80	2.99	3.00	3.03
o-xylene	3.47	1.84	1.68	1.63	2.41	2.43	2.42	2.59	2.57	2.58
naphthalene	2.92	2.24	2.14	2.13	2.02	2.02	2.04	2.17	2.14	2.14
MAE		0.53	0.60	0.61	0.87	0.88	0.89	0.72	0.75	0.76

[&]quot;Full stands for the full space. (20,20)/(30,30) means 20/30 occupied and virtual frontier orbitals are included in the active space. Geometries were taken from ref 76. Experimental values in the gas phase were taken as the reference values. The cc-pVDZ basis set was used. All values in eV.

Table 3. Double-Excitation Energies and MAEs of Small Molecules Obtained from the Full-Space and Active-Space ppRPA Approaches Based on HF, PBE, and B3LYP^a

			HF				PBE		B3LYP			
	state	ref	full	(30,30)	(20,20)	full	(30,30)	(20,20)	full	(30,30)	(20,20)	
Be	¹ D	7.05	7.06	7.03	7.03	7.61	7.69	7.70	7.96	8.05	8.07	
	^{3}P	7.40	7.45	7.46	7.47	7.49	7.52	7.54	7.84	7.88	7.90	
BH	$^3\Sigma$	5.04	5.52	5.46	5.41	4.89	4.84	4.80	5.12	5.07	5.02	
	$^{1}\Delta$	6.06	6.15	6.12	6.12	5.80	5.80	5.83	5.97	5.96	5.99	
	$^1\Sigma$	7.20	7.08	7.06	7.10	6.90	6.94	7.04	7.04	7.07	7.16	
butadiene	$^{1}A_{g}$	6.55	5.92	5.82	5.88	6.12	6.10	6.14	6.45	6.43	6.48	
hexatriene	$^{1}A_{g}$	5.21	5.43	5.38	5.39	4.49	4.48	4.48	5.00	4.99	5.01	
MAE			0.23	0.23	0.21	0.36	0.38	0.37	0.28	0.30	0.28	

^aFull stands for the full space. (20,20)/(30,30) means 20/30 occupied and virtual frontier orbitals are included in the active space. Geometries were optimized at the 6-31G*/MP2 level with the GAUSSIAN16 A.03 software. Reference values were taken from ref 43. The even-tempered basis set defined in ref 43 was used for Be and Li, the cc-pVQZ basis set was used for BH, the aug-cc-pVDZ basis set was used for C, and the cc-pVDZ basis set was used for H in polyenes. All values in eV.

virtual orbitals. However, as shown in eq 11, the size of the active space in ref 59 depends on the size of the full system. Therefore, the dimension can be large even with a small number of active orbitals. For the active space in this work, only particle and hole pairs with dominant contributions to the low-lying excitation energies are included, which lead to a small dimension. As shown in this work, only a constant number of orbitals are needed in the active space to provide converged excitation energies for systems of different sizes studied in this work. Therefore, the scaling to evaluate the required two-electron integrals is only $O(N_{\rm aux})$ by using RI, where $N_{\rm aux}$ is the number of the auxiliary system. Thus, the active-space ppRPA approach in this work is more efficient to predict excitation energies.

Excitation Energies from Active-Space ppRPA. S-T *Gaps of Diradicals.* We then examined the performance of the active-space ppRPA approach on calculating the S-T gaps of diradicals. The adiabatic S-T gaps and mean absolute errors (MAEs) of four diatomic diradicals and four carbene-like diradicals and the vertical S-T gaps of three disjoint diradicals and one four- π -electron diradical obtained from the full-space and active-space ppRPA approaches based on HF, PBE, and B3LYP are tabulated in Table 1. The vertical S-T gaps were

directly calculated as the difference between the two-electron addition energies of the singlet state and that of the triplet ground state. The adiabatic S-T gaps were obtained using the correction defined in eq 21. It can be seen that by using an active space consisting of 30 occupied and 30 virtual orbitals, the active-space ppRPA approach based on both HF and DFT references provides errors smaller than 0.3 kcal/mol compared with the full-space results, which are smaller than the errors of 1.0 kcal/mol by using the active space in ref 59. For carbenelike diradicals NH₂⁺, the error of the S-T gap for the 2¹A₁ state is 4.0 kcal/mol, which means the size of the active space needs to be increased for S-T gaps of high-lying states. As shown in Table 1, using an active-space consisting of a constant number of active orbitals, all S-T gaps obtained from the ppRPA approach have errors within 0.5 kcal/mol compared with the full-space results.

CT Excitation Energy. We further investigated the performance of the active-space ppRPA approach for predicting CT excitation energies. The first singlet excitation energies and MAEs of 12 intramolecular CT systems in the Stein CT test set obtained from the full-space and active-space ppRPA approaches based on HF, PBE, and B3LYP are tabulated in Table 2. It shows that the active-space ppRPA approach with

Table 4. Rydberg Excitation Energies and MAEs of Atomic Systems Obtained from the Full-Space and Active-Space ppRPA Approaches Based on HF, PBE, and B3LYP^a

			HF			PBE			B3LYP		
	state	ref	full	(30,30)	(20,20)	full	(30,30)	(20,20)	full	(30,30)	(20,20)
Be	triplet $2s \rightarrow 3s$	6.46	6.44	6.35	6.35	7.93	7.79	7.79	8.29	8.16	8.15
	singlet $2s \rightarrow 3s$	6.78	6.77	6.70	6.70	8.22	8.12	8.12	8.59	8.51	8.50
B^{+}	triplet $2s \rightarrow 3s$	16.09	16.06	15.95	15.96	18.60	18.45	18.46	18.51	18.37	18.39
	singlet $2s \rightarrow 3s$	17.06	17.09	17.28	17.34	19.42	19.41	19.47	19.49	19.56	19.65
Mg	triplet $3s \rightarrow 4s$	5.11	5.01	4.96	4.94	7.05	6.98	6.97	7.06	6.99	6.97
	singlet $3s \rightarrow 4s$	5.39	5.29	5.26	5.25	7.32	7.27	7.26	7.31	7.27	7.26
Al^+	triplet $3s \rightarrow 4s$	11.32	11.14	11.09	11.36	14.09	14.03	14.31	14.29	14.33	14.52
	singlet $3s \rightarrow 4s$	11.82	11.64	11.64	12.35	14.57	14.57	15.23	14.75	14.75	15.38
MAE			0.08	0.15	0.18	2.15	2.07	2.20	2.28	2.24	2.35

[&]quot;Full stands for the full space. (20,20)/(30,30) means 20/30 occupied and virtual frontier orbitals are included in the active space. Reference values were taken from ref 77. The aug-cc-pVQZ basis set was used. All values in eV.

an active space consisting of 30 occupied orbitals and 30 virtual orbitals provides errors smaller than 0.1 eV compared with the full-space ppRPA approach. The active-space ppRPA approach based on both the generalized gradient approximation (GGA) functional and the hybrid functional B3LYP has better convergence performance than that based on the HF reference, which has errors smaller than 0.03 eV. The slower convergence of ppRPA@HF can be attributed to the poor description for virtual orbitals by the HF reference. As discussed in ref 64, ppRPA@HF gives many excitations with incorrect symmetry below the targeted excitations, which also happens in TDHF and CIS calculations. Thus, ppRPA@HF needs a larger active space to get converged results of targeted excitations. As shown in Table 2, using an active space consisting of a constant number of active orbitals, all excitation energies of CT systems obtained from the active-space ppRPA@PBE and active-space ppRPA@B3LYP approaches have errors within 0.05 eV compared with the full-space results.

Double Excitations. We then move on to the performance of the active-space ppRPA approach for predicting double-excitation energies. The ppRPA approach can naturally describe the double-excitation energies. The double-excitation energies and MAEs of four molecules obtained from the full-space and active-space ppRPA approaches based on HF, PBE, and B3LYP are tabulated in Table 3. It shows that with an active space consisting of 30 occupied and 30 virtual orbitals, the active-space ppRPA approach based on all references provides errors smaller than 0.02 eV compared with the full-space results, which are smaller than the errors of 0.05 eV in ref 59. As shown in Table 3, an active space consisting a constant number of orbitals provides small errors for all tested systems.

Rydberg Excitations. We then evaluated the efficiency of the active-space ppRPA approach for predicting Rydberg excitation energies. The Rydberg excitation energies and MAEs of four atoms obtained from the full-space and active-space ppRPA approaches based on HF, PBE, and B3LYP are shown in Table 4. With an active space consisting of 30 occupied and 30 virtual orbitals, the active-space ppRPA approach based on all references provides errors smaller than 0.1 eV compared with the full space results, which is lower than the errors of 0.2 eV in ref 59. The active-space ppRPA@HF approach gives the smallest MAE around 0.15 eV because HF provides the correct long-range behavior for describing Rydberg states. Because Rydberg excitations are typically high-lying excited states, a larger active space is needed to obtain errors smaller than 0.05 eV. However, an active space containing a constant number of

orbitals provides errors smaller than 0.1 eV for all tested systems.

Valence Excitations. In this section, we investigate the effectiveness of the active-space ppRPA method in providing accurate valence excitation energies. The valence excitation energies and MAEs of molecules in the Thiel test set and the Tozer test set obtained from the full-space and active-space ppRPA approaches based on HF, PBE, and B3LYP are tabulated in Table 5. With an active space consisting of 30 occupied and 30 virtual orbitals, the active-space ppRPA approach based on the HF reference has errors larger than 0.5 eV. The active-space ppRPA approach based on different DFT references has much smaller MAEs about 0.03 eV compared with full-space results, which are smaller than the errors of 0.1 eV in ref 59. Results in Table 5 show that with DFT references, an active space consisting a constant number of orbitals provides errors around 0.05 eV for all tested systems.

S-T Gaps of Hydrocarbons. To demonstrate the performance of the active-space ppRPA approach, we calculated the S-T gaps of Chichibabin's hydrocarbon⁹⁷ and Müller's hydrocarbon⁹⁸ (as shown in Figure 2), which contain 66 atoms and 76 atoms, respectively. These two hydrocarbons show a strong reactivity and diradical characteristic because of the formation of aromatic rings. 99 Müller's hydrocarbon is expected to have a stronger diradical characteristic and a smaller S-T gap than those of Chichibabin's hydrocarbon because it has one more aromatic ring. 84,86,99 The S-T gaps and the dominant configuration contributions (DCCs) of two hydrocarbons obtained from the active-space ppRPA@B3LYP approach with the cc-pVDZ basis set are shown in Table 6. 30 occupied and 30 virtual orbitals are included in the active space. As shown in Table S1 in the Supporting Information, for the studied hydrocarbon systems that have around 80 atoms, using the active space with 30 occupied and virtual orbitals provides the converged results, which is the same as small atomic systems. This further suggests that the dimension of the active space is independent of the size of the system for lowlying excitations based on the results of the systems studied. The calculated S-T gap of Chichibabin's hydrocarbon is -3.0kcal/mol, which is close to the experimental value of -5.5kcal/mol in ref 85. The active-space ppRPA approach predicts a smaller S-T gap of -0.1 kcal/mol for Müller's hydrocarbon, which is similar to the reference value of -0.3 kcal/mol in ref 86. Then, we investigated the diradical characteristic of these two hydrocarbons by analyzing the DCC. As shown in ref 58, the larger the DCC, the less the diradical characteristic. For

Table 5. Valence Excitation Energies and MAEs of the Thiel Test Set^{78,79} and the Tozer Test Set⁸⁰ Energies Obtained from the Full-Space and Active-Space ppRPA Approaches Based on HF, PBE, and B3LYP^a

				HF			PBE			B3LYP	
	state	ref	full	(30,30)	(20,20)	full	(30,30)	(20,20)	full	(30,30)	(20,20)
ethene	$^3B_{1u}$	4.50	3.92	3.81	3.76	3.48	3.40	3.40	3.62	3.53	3.52
ethene	$^{1}\mathrm{B}_{1\mathrm{u}}$	7.80	6.25	6.02	5.88	8.86	8.93	9.09	8.46	8.43	8.31
butadiene	$^{3}B_{u}$	3.20	3.21	3.13	3.13	2.28	2.20	2.23	2.52	2.44	2.46
butadiene	$^{3}A_{g}$	5.08	5.60	5.27	5.47	5.85	5.82	5.87	6.07	6.03	6.09
butadiene	$^{1}B_{u}$	6.18	5.49	4.55	4.56	6.52	6.76	6.92	6.58	6.77	6.85
butadiene	$^{1}A_{g}$	6.55	5.92	5.27	5.43	6.11	6.09	6.14	6.44	6.42	6.47
hexatriene	$^{3}B_{u}$	2.40	2.58	2.53	2.57	1.61	1.56	1.55	1.88	1.83	1.83
hexatriene	$^{3}A_{g}$	4.15	5.20	3.90	3.98	4.47	4.46	4.46	4.86	4.86	4.87
hexatriene	$^{1}A_{g}$	5.09	5.42	3.92	4.00	4.49	4.48	4.47	4.99	4.99	4.99
hexatriene	$^{1}B_{\mathrm{u}}$	5.10	5.04	4.09	4.08	5.14	5.29	5.38	5.30	5.44	5.55
octatetraene	$^{3}B_{\mathrm{u}}$	2.20	2.15	2.10	2.10	1.21	1.18	1.16	1.49	1.46	1.44
octatetraene	$^{3}A_{g}$	3.55	4.75	3.69	3.75	3.57	3.55	3.54	4.00	3.99	3.99
octatetraene	$^{1}A_{g}$	4.47	5.02	3.70	3.77	3.53	3.52	3.51	4.08	4.07	4.07
octatetraene	$^{1}B_{\mathrm{u}}$	4.66	4.58	3.78	3.77	4.30	4.44	4.47	4.50	4.65	4.65
cyclopropene	${}^{3}B_{2}$	4.34	4.22	4.08	4.05	3.91	3.86	3.85	4.08	4.03	4.01
cyclopropene	$^{1}B_{2}$	7.06	5.87	4.29	4.22	7.33	7.50	7.54	7.31	7.44	7.46
cyclopentadiene	${}^{3}B_{2}$	3.25	3.12	3.02	2.99	2.52	2.46	2.49	2.66	2.58	2.62
cyclopentadiene	${}^{3}A_{1}$	5.09	5.45	3.16	3.12	5.07	5.04	5.10	5.32	5.29	5.38
cyclopentadiene	${}^{1}B_{2}$	5.55	5.16	3.19	3.15	5.46	5.68	5.96	5.47	5.68	5.79
cyclopentadiene	$^{1}A_{1}$	6.31	6.01	3.64	3.80	6.16	6.18	6.26	6.42	6.44	6.55
norbornadiene	3 A ₂	3.72	3.77	3.39	3.50	3.58	3.57	3.54	3.68	3.66	3.64
norbornadiene	${}^{3}B_{2}$	4.16	4.48	3.64	3.75	4.51	4.49	4.45	4.75	4.72	4.68
norbornadiene	${}^{1}A_{2}$	5.34	3.95	3.41	3.54	5.35	5.52	5.72	5.36	5.54	5.71
norbornadiene	$^{1}B_{2}$	6.11	4.58	3.91	4.21	7.00	7.12	7.25	6.78	6.69	6.90
furan	${}^{3}B_{2}$	4.17	3.82	3.65	3.64	3.37	3.29	3.30	3.49	3.41	3.41
furan	${}^{3}A_{1}$	5.48	5.78	3.69	3.72	5.12	5.07	5.13	5.37	5.32	5.39
furan	${}^{1}B_{2}$	6.32	5.09	3.68	3.67	6.58	6.69	6.82	6.50	6.38	6.42
furan	$^{1}A_{1}$	6.57	6.61	4.08	4.08	6.65	6.75	6.82	6.88	6.91	7.09
s-tetrazine	$^{3}\mathrm{B}_{\mathrm{3u}}$	1.89	3.28	3.24	3.28	1.86	1.82	1.85	2.19	2.14	2.18
s-tetrazine	$^{3}A_{u}$	3.52	5.38	5.32	5.38	3.16	3.12	3.09	3.67	3.62	3.61
s-tetrazine	$^{1}\mathrm{B}_{3\mathrm{u}}$	2.24	3.78	3.77	3.85	2.41	2.42	2.45	2.73	2.73	2.78
s-tetrazine	$^{1}A_{u}$	3.48	5.60	5.55	5.64	3.40	3.37	3.35	3.91	3.87	3.87
formaldehyde	$^{3}A_{2}$	3.50	1.66	1.50	1.39	3.41	3.32	3.26	3.15	3.05	2.98
formaldehyde	${}^{1}A_{2}$	3.88	2.00	1.85	1.75	3.97	3.90	3.85	3.68	3.60	3.54
acetone	$^{3}A_{2}$	4.05	3.10	2.36	2.30	4.24	4.17	4.29	4.14	4.04	4.18
acetone	${}^{1}A_{2}$	4.40	3.38	2.39	2.34	4.66	4.59	4.72	4.55	4.46	4.62
benzoquinone	$^{3}\mathrm{B}_{1\mathrm{g}}$	2.51	4.75	4.76	4.76	2.45	2.45	2.47	2.93	2.94	2.95
benzoquinone	$^{1}\mathrm{B}_{1\mathrm{g}}$	2.78	4.98	5.02	5.02	2.65	2.67	2.70	3.14	3.17	3.19
MAE			0.85	1.36	1.36	0.39	0.42	0.46	0.37	0.39	0.43

"Full stands for the full space. (20,20)/(30,30) means 20/30 occupied and virtual frontier orbitals are included in the active space. Geometries and reference values were taken from refs 78–80. The aug-cc-pVDZ basis set was used. All values in eV.

Figure 2. Structures of hydrocarbons. n = 2: Chichibabin's hydrocarbon. n = 3: Müller's hydrocarbon.

Chichibabin's hydrocarbon, the configuration with two electrons occupying the HOMO contributes 66.7% to singlet ground state. For Müller's hydrocarbon, the configuration with two electrons occupying the HOMO contributes 54.6% to singlet ground state, which shows a much stronger diradical characteristic.

By using the active-space ppRPA approach, the above calculations for two large hydrocarbons can be efficiently performed. For example, the restricted calculation for Müller's hydrocarbon with the cc-pVDZ basis set contains 147 occupied orbitals and 673 virtual orbitals. The dimension of the full-space ppRPA matrix for the singlet calculation is 237,679. In the active-space ppRPA approach with 30 active occupied orbitals and 30 active virtual orbitals, the dimension is reduced to 930. The computational cost is greatly reduced compared with the full-space calculation.

CLBEs Obtained from Active-Space T-Matrix Approaches. The performance of the active-space T-matrix approach on predicting QP energies is discussed in this section. The active-space $G_{\rm RS}T_{\rm RS}$ approach was used to

Table 6. S-T Gaps and the Dominant Configuration Contributions of Chichibabin's Hydrocarbon and Müller's Hydrocarbon Obtained from the Active-Space ppRPA Approaches Based on B3LYP^a

	ΔE_{S-T} ref (kcal/mol)	$\Delta E_{\mathrm{S-T}}$ calc (kcal/mol)	HOMO + HOMO (%)	LUMO + LUMO (%)
Chichibabin	-5.5	-3.0	66.9	28.5
Müller	-0.3	-0.1	54.6	42.5

^a30 occupied and 30 virtual frontier orbitals are included in the active space. Geometries were taken from ref 84. Reference values were taken from refs 85 and 86. The cc-pVDZ basis set was used.

calculate the QP energies. The $G_{\rm RS}T_{\rm RS}$ approach that uses the RS Green's function as the starting point and formulates the effective interaction is shown to predict accurate valence and core QP energies. As shown in Figure S1 in the Supporting Information, the active-space T-matrix approach needs around 50% orbitals in the active space to obtain ionization potentials (IPs) with errors smaller than 0.05 eV. However, for predicting CLBEs, the active-space T-matrix approach with the active space consisting of only all occupied orbitals produces errors smaller than 0.1 eV, which corresponds to a percent error of 0.02%. Thus, we focus on predicting CLBEs with the active-space T-matrix approach.

The MAEs of absolute and relative CLBEs obtained from the active-space $G_{\rm RS}T_{\rm RS}$ and G_0T_0 approach based on HF, PBE, and B3LYP are shown in Tables 7 and 8. For absolute CLBEs,

Table 7. MAEs of Absolute CLBEs in the CORE65 Set Obtained from the Full-Space and Active-Space and G_0T_0 and $G_{\rm RS}T_{\rm RS}$ Approaches Based on HF, PBE, and B3LYP^a

		HF	PBE	B3LYP
G_0T_0	full-space	3.74	14.97	9.34
	active-space	3.81	14.58	9.43
$G_{ m RS}T_{ m RS}$	full-space	3.74	1.53	1.66
	active-space	3.81	1.58	1.68

"Only occupied orbitals are in the active space. The NIP approximation is used to approximate the contribution to the self-energy outside the active space. Full-space results were taken from ref 68. Geometries and reference values were taken from the CORE65 set. The def2-TZVP basis set was used. All values in eV.

the active-space G_0T_0 approach has errors of around 0.1 to 0.5 eV compared with the full-space results. The active-space $G_{\rm RS}T_{\rm RS}$ approach produces errors smaller than 0.1 eV compared with the full-space results. The active-space $G_{\rm RS}T_{\rm RS}$ @PBE approach has the smallest MAE of 1.58 eV compared with reference values, which agrees with the full-space results. For relative CLBEs, the active-space G_0T_0 approach leads to large errors around 0.1 to 0.5 eV compared with the full-space results. The active-space $G_{\rm RS}T_{\rm RS}$ approach

provides errors only around 0.03 eV. The active-space $G_{\rm RS}T_{\rm RS}$ @PBE approach has the smallest MAEs compared with reference values, which agree with the full-space results. Therefore, the active-space $G_{\rm RS}T_{\rm RS}$ approach is promising for predicting absolute and relative CLBEs by using an active space consisting of only occupied orbitals and the NIP approximation.

CONCLUSIONS

In summary, we developed a new efficient active-space ppRPA approach to predict accurate excitation energies of molecular systems. In the active-space ppRPA approach, both indexes in particle and hole pairs are constrained, which only includes the particle and hole pairs with large contributions to low-lying excitation energies. We showed that by using the active space composed of only 30 occupied and 30 virtual orbitals, the active-space ppRPA approach produces errors smaller than 0.05 eV compared with the full-space results for excitations of different characteristics, including CT, Rydberg, double, valence, and diradical excitations. Therefore, the scaling of the active-space ppRPA approach is only O(N), which is much lower than $O(N^3)$ in the previous work. In contrast to the commonly used particle-hole RPA or TDDFT, in which there is no known way to explore the active space in the molecular orbital space, ppRPA, as we have shown, allows direct truncation of the molecular orbitals to form a much smaller active space, leading to our efficient solution to the low-lying excitation energies. As shown in this work and the previous works, ppRPA with conventional functionals provides accurate excitation energies for Rydberg and diradical excitations. However, the accuracy for predicting valence excitation energies is slightly worse compared with TDDFT with hybrid functionals. The performance benchmark of the ppRPA approach with other DFAs will be investigated in the future work. We show that the dimension of the active space that provides converged excitation energies is independent of the system size. Furthermore, the size of the active space needed for different systems can be tested easily for convergence. We also combined the active-space ppRPA approach with the NIP

Table 8. MAEs of Relative CLBEs in the CORE65 Set Obtained from the Full-Space and Active-Space and G_0T_0 and $G_{RS}T_{RS}$ Approaches Based on HF, PBE, and B3LYP^a

	full-space G_0T_0			active-space G_0T_0			full-space $G_{ m RS}T_{ m RS}$			active-space $G_{RS}T_{RS}$		
	HF	PBE	B3LYP	HF	PBE	B3LYP	HF	PBE	B3LYP	HF	PBE	B3LYP
С	0.33	0.85	0.41	0.27	1.37	0.82	0.33	0.39	0.46	0.27	0.32	0.45
N	0.09	1.40	0.88	0.23	1.71	1.07	0.09	0.19	0.12	0.23	0.22	0.15
O	0.22	2.29	1.47	0.29	2.21	1.46	0.22	0.29	0.27	0.29	0.25	0.25
F	0.13	0.22	0.11	0.14	0.22	0.13	0.13	0.22	0.07	0.14	0.21	0.24

^aThe relative CLBEs are the shifts with respect to a reference molecule, Δ CLBE = CLBE – CLBE_{ref}. CH₄, NH₃, H2O, and CF4 have been used as reference molecules for C 1s, N 1s, O 1s, and F 1s, respectively. Only occupied orbitals are included in the active space. The NIP approximation is used to approximate the contribution to the self-energy outside the active space. Full-space results were taken from ref 68. Geometries and reference values were taken from the CORE65 set.⁸⁷ The def2-TZVP basis set was used. All values in eV.

approximation in the T-matrix approximation to compute QP energies. The NIP approximation uses KS orbital energies and orbitals to approximate the contribution to the self-energy outside the self-energy. In the active-space T-matrix approach, by using the active space only consisting of occupied orbitals, the computational cost to evaluate the self-energy in the active space becomes $O(N^6)$ with a very small prefactor and outside the active space becomes $O(N^5)$. The active-space $G_{\rm RS}T_{\rm RS}$ approach predicts accurate absolute and relative CLBEs with the MAE around 1.5 and 0.3 eV, respectively. The active-space formalism is expected to greatly extend the applicability of the ppRPA and T-matrix approaches for large systems.

ASSOCIATED CONTENT

Data Availability Statement

Data and scripts pertaining to this work have been archived in the Duke Research Data Repository. 100

Supporting Information

The Supporting Information is available free of charge at https://pubs.acs.org/doi/10.1021/acs.jpca.3c02834.

Convergence behavior of the active-space T-matrix approach, convergence behavior of the active-space ppRPA approach for hydrocarbon molecules, and numerical results of CLBEs obtained from active-space T-matrix approaches (PDF)

AUTHOR INFORMATION

Corresponding Author

Weitao Yang — Department of Chemistry, Duke University, Durham, North Carolina 27708, United States;

orcid.org/0000-0001-5576-2828; Email: weitao.yang@duke.edu

Authors

Jiachen Li — Department of Chemistry, Duke University, Durham, North Carolina 27708, United States;
orcid.org/0000-0002-9863-1091

Jincheng Yu − Department of Chemistry, Duke University, Durham, North Carolina 27708, United States; orcid.org/0000-0001-8487-5565

Zehua Chen — Department of Chemistry, Duke University, Durham, North Carolina 27708, United States; orcid.org/0000-0002-1839-5034

Complete contact information is available at: https://pubs.acs.org/10.1021/acs.jpca.3c02834

Notes

The authors declare no competing financial interest.

ACKNOWLEDGMENTS

We acknowledge the support from the National Institutes of Health under award number R01-GM061870 (J.L., J.Y., and Z.C.) and the National Science Foundation (grant no. CHE-2154831) (W.Y.).

REFERENCES

- (1) Casida, M. E. Recent Advances in Density Functional Methods. In *Recent Advances in Computational Chemistry*; World Scientific, 1995; Vol. 1, pp 155–192.
- (2) Ullrich, C. A. Time-Dependent Density-Functional Theory: Concepts and Applications; OUP Oxford, 2011.

- (3) Runge, E.; Gross, E. K. U. Density-Functional Theory for Time-Dependent Systems. *Phys. Rev. Lett.* **1984**, *52*, 997–1000.
- (4) Casida, M.; Ipatov, A.; Cordova, F.. In *Time-Dependent Density Functional Theory*; Marques, M. A., Ullrich, C. A., Nogueira, F., Rubio, A., Burke, K., Gross, E. K. U., Eds.; *Lecture Notes in Physics*; Springer: Berlin, Heidelberg, 2006; pp 243–257.
- (5) Casida, M. E. Time-Dependent Density-Functional Theory for Molecules and Molecular Solids. *J. Mol. Struct.* **2009**, *914*, 3–18.
- (6) Laurent, A. D.; Jacquemin, D. TD-DFT Benchmarks: A Review. Int. J. Quantum Chem. 2013, 113, 2019–2039.
- (7) Tozer, D. J. Relationship between Long-Range Charge-Transfer Excitation Energy Error and Integer Discontinuity in Kohn-Sham Theory. J. Chem. Phys. 2003, 119, 12697–12699.
- (8) Dreuw, A.; Weisman, J. L.; Head-Gordon, M. Long-Range Charge-Transfer Excited States in Time-Dependent Density Functional Theory Require Non-Local Exchange. *J. Chem. Phys.* **2003**, *119*, 2943–2946.
- (9) Leininger, T.; Stoll, H.; Werner, H.-J.; Savin, A. Combining Long-Range Configuration Interaction with Short-Range Density Functionals. *Chem. Phys. Lett.* **1997**, 275, 151–160.
- (10) Besley, N. A.; Peach, M. J. G.; Tozer, D. J. Time-Dependent Density Functional Theory Calculations of near-Edge X-ray Absorption Fine Structure with Short-Range Corrected Functionals. *Phys. Chem. Phys.* **2009**, *11*, 10350–10358.
- (11) Stein, T.; Kronik, L.; Baer, R. Prediction of Charge-Transfer Excitations in Coumarin-Based Dyes Using a Range-Separated Functional Tuned from First Principles. *J. Chem. Phys.* **2009**, *131*, 244119.
- (12) Refaely-Abramson, S.; Baer, R.; Kronik, L. Fundamental and Excitation Gaps in Molecules of Relevance for Organic Photovoltaics from an Optimally Tuned Range-Separated Hybrid Functional. *Phys. Rev. B* **2011**, *84*, 075144.
- (13) Brückner, C.; Engels, B. Benchmarking Singlet and Triplet Excitation Energies of Molecular Semiconductors for Singlet Fission: Tuning the Amount of HF Exchange and Adjusting Local Correlation to Obtain Accurate Functionals for Singlet—Triplet Gaps. *Chem. Phys.* **2017**, *482*, 319—338.
- (14) Gong, J.; Lam, Y.; Tang, B. Z.; Zhong Tang, B. Benchmark and Parameter Tuning of Hybrid Functionals for Fast Calculation of Excitation Energies of AIEgens. *Phys. Chem. Chem. Phys.* **2020**, 22, 18035–18039.
- (15) Kempfer-Robertson, E. M.; Haase, M. N.; Bersson, J. S.; Avdic, I.; Thompson, L. M. Role of Exact Exchange in Difference Projected Double-Hybrid Density Functional Theory for Treatment of Local, Charge Transfer, and Rydberg Excitations. *J. Phys. Chem. A* **2022**, *126*, 8058–8069.
- (16) Sham, L. J.; Rice, T. M. Many-Particle Derivation of the Effective-Mass Equation for the Wannier Exciton. *Phys. Rev.* **1966**, 144, 708–714.
- (17) Hanke, W.; Sham, L. J. Many-Particle Effects in the Optical Excitations of a Semiconductor. *Phys. Rev. Lett.* **1979**, *43*, 387–390.
- (18) Salpeter, E. E.; Bethe, H. A. A Relativistic Equation for Bound-State Problems. *Phys. Rev.* **1951**, *84*, 1232–1242.
- (19) Golze, D.; Dvorak, M.; Rinke, P. The GW compendium: A practical guide to theoretical photoemission spectroscopy. *Front. Chem.* **2019**, *7*, 377.
- (20) Martin, R. M.; Reining, L.; Ceperley, D. M. *Interacting Electrons*; Cambridge University Press, 2016.
- (21) Reining, L. The GW Approximation: Content, Successes and Limitations. Wiley Interdiscip. Rev. Comput. Mol. Sci. 2018, 8, No. e1344.
- (22) Hedin, L. New Method for Calculating the One-Particle Green's Function with Application to the Electron-Gas Problem. *Phys. Rev.* **1965**, *139*, A796–A823.
- (23) Yao, Y.; Golze, D.; Rinke, P.; Blum, V.; Kanai, Y. All-electron BSE@ GW method for K-edge core electron excitation energies. *J. Chem. Theory Comput.* **2022**, *18*, 1569–1583.
- (24) McKeon, C. A.; Hamed, S. M.; Bruneval, F.; Neaton, J. B. An Optimally Tuned Range-Separated Hybrid Starting Point for Ab

- Initio GW plus Bethe-Salpeter Equation Calculations of Molecules. J. Chem. Phys. 2022, 157, 074103.
- (25) Knysh, I.; Duchemin, I.; Blase, X.; Jacquemin, D. Modeling of excited state potential energy surfaces with the Bethe–Salpeter equation formalism: The 4-(dimethylamino) benzonitrile twist. *J. Chem. Phys.* **2022**, *157*, 157.
- (26) Balasubramani, S. G.; Voora, V. K.; Furche, F. Static polarizabilities within the generalized Kohn–Sham semicanonical projected random phase approximation (GKS-spRPA). *J. Chem. Phys.* **2022**, *157*, 157.
- (27) Li, J.; Golze, D.; Yang, W. Combining Renormalized Singles GW Methods with the Bethe-Salpeter Equation for Accurate Neutral Excitation Energies. *J. Chem. Theory Comput.* **2022**, *18*, 6637–6645.
- (28) Marom, N.; Caruso, F.; Ren, X.; Hofmann, O. T.; Körzdörfer, T.; Chelikowsky, J. R.; Rubio, A.; Scheffler, M.; Rinke, P. Benchmark of GW Methods for Azabenzenes. *Phys. Rev. B* **2012**, *86*, 245127.
- (29) Duchemin, I.; Blase, X. Cubic-Scaling All-Electron GW Calculations with a Separable Density-Fitting Space—Time Approach. *J. Chem. Theory Comput.* **2021**, *17*, 2383—2393.
- (30) Förster, A.; Visscher, L. Quasiparticle Self-Consistent GW-Bethe-Salpeter Equation Calculations for Large Chromophoric Systems. *J. Chem. Theory Comput.* **2022**, *18*, 6779–6793.
- (31) Jacquemin, D.; Duchemin, I.; Blondel, A.; Blase, X. Benchmark of Bethe-Salpeter for Triplet Excited-States. *J. Chem. Theory Comput.* **2017**, *13*, 767–783.
- (32) Li, J.; Jin, Y.; Su, N. Q.; Yang, W. Combining Localized Orbital Scaling Correction and Bethe–Salpeter Equation for Accurate Excitation Energies. *J. Chem. Phys.* **2022**, *156*, 154101.
- (33) Elliott, J. D.; Colonna, N.; Marsili, M.; Marzari, N.; Umari, P. Koopmans Meets Bethe—Salpeter: Excitonic Optical Spectra without GW. J. Chem. Theory Comput. 2019, 15, 3710–3720.
- (34) Loos, P.-F.; Romaniello, P. Static and Dynamic Bethe—Salpeter Equations in the T-matrix Approximation. *J. Chem. Phys.* **2022**, *156*, 164101.
- (35) Andersson, K.; Malmqvist, P.-Å.; Roos, B. O. Second-order Perturbation Theory with a Complete Active Space Self-consistent Field Reference Function. *J. Chem. Phys.* **1992**, *96*, 1218–1226.
- (36) Christiansen, O.; Koch, H.; Jo/rgensen, P. Response Functions in the CC3 Iterative Triple Excitation Model. *J. Chem. Phys.* **1995**, 103, 7429–7441.
- (37) Koch, H.; Jensen, H. J. A.; Jo/rgensen, P.; Helgaker, T. Excitation Energies from the Coupled Cluster Singles and Doubles Linear Response Function (CCSDLR). Applications to Be, CH+, CO, and H2O. *J. Chem. Phys.* **1990**, *93*, 3345–3350.
- (38) Loos, P.-F.; Scemama, A.; Blondel, A.; Garniron, Y.; Caffarel, M.; Jacquemin, D. A Mountaineering Strategy to Excited States: Highly Accurate Reference Energies and Benchmarks. *J. Chem. Theory Comput.* **2018**, *14*, 4360–4379.
- (39) Loos, P.-F.; Lipparini, F.; Boggio-Pasqua, M.; Scemama, A.; Jacquemin, D. A Mountaineering Strategy to Excited States: Highly Accurate Energies and Benchmarks for Medium Sized Molecules. *J. Chem. Theory Comput.* **2020**, *16*, 1711–1741.
- (40) Véril, M.; Scemama, A.; Caffarel, M.; Lipparini, F.; Boggio-Pasqua, M.; Jacquemin, D.; Loos, P.-F. QUESTDB: A Database of Highly Accurate Excitation Energies for the Electronic Structure Community. Wiley Interdiscip. Rev.: Comput. Mol. Sci. 2021, 11, No. e1517.
- (41) Ring, P.; Schuck, P. The nuclear many-body problem; Springer Science & Business Media, 2004.
- (42) Ripka, S. R. P. G.; Blaizot, J.-P.; Ripka, G. Quantum Theory of Finite Systems; MIT Press, 1986.
- (43) Yang, Y.; van Aggelen, H.; Yang, W. Double, Rydberg and Charge Transfer Excitations from Pairing Matrix Fluctuation and Particle-Particle Random Phase Approximation. *J. Chem. Phys.* **2013**, 139. 224105.
- (44) van Aggelen, H.; Yang, Y.; Yang, W. Exchange-Correlation Energy from Pairing Matrix Fluctuation and the Particle-Particle Random-Phase Approximation. *Phys. Rev. A* **2013**, *88*, 030501.

- (45) van Aggelen, H.; Yang, Y.; Yang, W. Exchange-Correlation Energy from Pairing Matrix Fluctuation and the Particle-Particle Random Phase Approximation. *J. Chem. Phys.* **2014**, *140*, 18A511.
- (46) Langreth, D. C.; Perdew, J. P. Exchange-Correlation Energy of a Metallic Surface: Wave-vector Analysis. *Phys. Rev. B* **1977**, *15*, 2884–2901.
- (47) Harris, J.; Jones, R. O. The Surface Energy of a Bounded Electron Gas. J. Phys. F: Met. Phys. 1974, 4, 1170-1186.
- (48) Peng, D.; van Aggelen, H.; Yang, Y.; Yang, W. Linear-Response Time-Dependent Density-Functional Theory with Pairing Fields. *J. Chem. Phys.* **2014**, *140*, 18A522.
- (49) Ring, P.; Schuck, P. The Nuclear Many-Body Problem; Springer-Verlag: New York, 1980.
- (50) Rowe, D. J. Equations-of-Motion Method and the Extended Shell Model. Rev. Mod. Phys. 1968, 40, 153-166.
- (51) Bohm, D.; Pines, D. A Collective Description of Electron Interactions. I. Magnetic Interactions. *Phys. Rev.* **1951**, 82, 625–634.
- (52) Ren, X.; Rinke, P.; Joas, C.; Scheffler, M. Random-Phase Approximation and Its Applications in Computational Chemistry and Materials Science. *J. Mater. Sci.* **2012**, *47*, 7447–7471.
- (53) Bannwarth, C.; Yu, J. K.; Hohenstein, E. G.; Martínez, T. J. Hole–Hole Tamm–Dancoff-approximated Density Functional Theory: A Highly Efficient Electronic Structure Method Incorporating Dynamic and Static Correlation. *J. Chem. Phys.* **2020**, *153*, 024110.
- (54) Yu, J. K.; Bannwarth, C.; Hohenstein, E. G.; Martínez, T. J. Ab Initio Nonadiabatic Molecular Dynamics with Hole–Hole Tamm–Dancoff Approximated Density Functional Theory. *J. Chem. Theory Comput.* **2020**, *16*, 5499–5511.
- (55) Yang, Y.; Shen, L.; Zhang, D.; Yang, W. Conical Intersections from Particle—Particle Random Phase and Tamm—Dancoff Approximations. *J. Phys. Chem. Lett.* **2016**, *7*, 2407–2411.
- (56) Hohenberg, P.; Kohn, W. Inhomogeneous Electron Gas. *Phys. Rev.* **1964**, *136*, B864–B871.
- (57) Parr, R. G.; Weitao, Y. Density-Functional Theory of Atoms and Molecules; Oxford University Press, 1989.
- (58) Yang, Y.; Davidson, E. R.; Yang, W. Nature of Ground and Electronic Excited States of Higher Acenes. *Proc. Natl. Acad. Sci. U.S.A.* **2016**, *113*, E5098–E5107.
- (59) Zhang, D.; Yang, W. Accurate and Efficient Calculation of Excitation Energies with the Active-Space Particle-Particle Random Phase Approximation. *J. Chem. Phys.* **2016**, *145*, 144105.
- (60) Yang, Y.; Peng, D.; Davidson, E. R.; Yang, W. Singlet-Triplet Energy Gaps for Diradicals from Particle-Particle Random Phase Approximation. *J. Phys. Chem. A* **2015**, *119*, 4923–4932.
- (61) Strinati, G. Application of the Green's Functions Method to the Study of the Optical Properties of Semiconductors. *Riv. Nuovo Cimento* 1988, 11, 1–86.
- (62) Lu, J.; Yang, H. A Cubic Scaling Algorithm for Excited States Calculations in Particle—Particle Random Phase Approximation. *J. Comput. Phys.* **2017**, 340, 297–308.
- (63) Yang, Y.; Dominguez, A.; Zhang, D.; Lutsker, V.; Niehaus, T. A.; Frauenheim, T.; Yang, W. Charge Transfer Excitations from Particle-Particle Random Phase Approximation—Opportunities and Challenges Arising from Two-Electron Deficient Systems. *J. Chem. Phys.* 2017, 146, 124104.
- (64) Yang, Y.; Peng, D.; Lu, J.; Yang, W. Excitation Energies from Particle-Particle Random Phase Approximation: Davidson Algorithm and Benchmark Studies. *J. Chem. Phys.* **2014**, *141*, 124104.
- (65) Chen, Z.; Zhang, D.; Jin, Y.; Yang, Y.; Su, N. Q.; Yang, W. Multireference Density Functional Theory with Generalized Auxiliary Systems for Ground and Excited States. *J. Phys. Chem. Lett.* **2017**, *8*, 4479–4485.
- (66) Li, J.; Chen, Z.; Yang, W. Multireference Density Functional Theory for Describing Ground and Excited States with Renormalized Singles. *J. Phys. Chem. Lett.* **2022**, *13*, 894–903.
- (67) Zhang, D.; Su, N. Q.; Yang, W. Accurate Quasiparticle Spectra from the T-Matrix Self-Energy and the Particle—Particle Random Phase Approximation. *J. Phys. Chem. Lett.* **2017**, *8*, 3223–3227.

- (68) Li, J.; Chen, Z.; Yang, W. Renormalized Singles Green's Function in the T-Matrix Approximation for Accurate Quasiparticle Energy Calculation. *J. Phys. Chem. Lett.* **2021**, *12*, 6203–6210.
- (69) Davidson, E. R. The Iterative Calculation of a Few of the Lowest Eigenvalues and Corresponding Eigenvectors of Large Real-Symmetric Matrices. *J. Comput. Phys.* **1975**, *17*, 87–94.
- (70) Jin, Y.; Su, N. Q.; Yang, W. Renormalized Singles Green's Function for Quasi-Particle Calculations beyond the G0W0 Approximation. J. Phys. Chem. Lett. 2019, 10, 447–452.
- (71) Li, J.; Jin, Y.; Rinke, P.; Yang, W.; Golze, D. Benchmark of GW Methods for Core-Level Binding Energies. *J. Chem. Theory Comput.* **2022**, *18*, 7570–7585.
- (72) Li, J.; Yang, W. Renormalized Singles with Correlation in GW Green's Function Theory for Accurate Quasiparticle Energies. *J. Phys. Chem. Lett.* **2022**, *13*, 9372–9380.
- (73) Tahir, M. N.; Ren, X. Comparing Particle-Particle and Particle-Hole Channels of the Random Phase Approximation. *Phys. Rev. B* **2019**, *99*, 195149.
- (74) Yang, Y.; van Aggelen, H.; Steinmann, S. N.; Peng, D.; Yang, W. Benchmark Tests and Spin Adaptation for the Particle-Particle Random Phase Approximation. *J. Chem. Phys.* **2013**, *139*, 174110.
- (75) See http://www.qm4d.info for an in-house program for QM/MM simulations. (Accessed 2023/05/01).
- (76) Stein, T.; Kronik, L.; Baer, R. Reliable Prediction of Charge Transfer Excitations in Molecular Complexes Using Time-Dependent Density Functional Theory. J. Am. Chem. Soc. 2009, 131, 2818–2820.
- (77) Xu, X.; Yang, K. R.; Truhlar, D. G. Testing Noncollinear Spin-Flip, Collinear Spin-Flip, and Conventional Time-Dependent Density Functional Theory for Predicting Electronic Excitation Energies of Closed-Shell Atoms. *J. Chem. Theory Comput.* **2014**, *10*, 2070–2084.
- (78) Silva-Junior, M. R.; Schreiber, M.; Sauer, S. P. A.; Thiel, W. Benchmarks for Electronically Excited States: Time-dependent Density Functional Theory and Density Functional Theory Based Multireference Configuration Interaction. *J. Chem. Phys.* **2008**, *129*, 104103.
- (79) Schreiber, M.; Silva-Junior, M. R.; Sauer, S. P. A.; Thiel, W. Benchmarks for Electronically Excited States: CASPT2, CC2, CCSD, and CC3. *J. Chem. Phys.* **2008**, *128*, 134110.
- (80) Peach, M. J. G.; Benfield, P.; Helgaker, T.; Tozer, D. J. Excitation Energies in Density Functional Theory: An Evaluation and a Diagnostic Test. J. Chem. Phys. 2008, 128, 044118.
- (81) Dunning, T. H. Gaussian Basis Sets for Use in Correlated Molecular Calculations. I. The Atoms Boron through Neon and Hydrogen. *J. Chem. Phys.* **1989**, *90*, 1007–1023.
- (82) Kendall, R. A.; Dunning, T. H.; Harrison, R. J. Electron affinities of the first-row atoms revisited. Systematic basis sets and wave functions. *J. Chem. Phys.* **1992**, *96*, *6796*–*6806*.
- (83) Frisch, M. J.; Trucks, G. W.; Schlegel, H. B.; Scuseria, G. E.; Robb, M. A.; Cheeseman, J. R.; Scalmani, G.; Barone, V.; Petersson, G. A.; Nakatsuji, H.; et al. *Gaussian16*. Revision A.03; Gaussian Inc: Wallingford CT, 2016;.
- (84) Escayola, S.; Callís, M.; Poater, A.; Solà, M. Effect of Exocyclic Substituents and π -System Length on the Electronic Structure of Chichibabin Diradical(Oid)s. ACS Omega 2019, 4, 10845–10853.
- (85) Montgomery, L. K.; Huffman, J. C.; Jurczak, E. A.; Grendze, M. P. The Molecular Structures of Thiele's and Chichibabin's Hydrocarbons. *J. Am. Chem. Soc.* **1986**, *108*, 6004–6011.
- (86) Schmidt, R.; Brauer, H.-D. The Energetic Positions of the Lowest Singlet and Triplet State of the Schlenk and of the Müller Hydrocarbon. *Angew Chem. Int. Ed. Engl.* **1971**, *10*, 506–507.
- (87) Golze, D.; Keller, L.; Rinke, P. Accurate Absolute and Relative Core-Level Binding Energies from GW. *J. Phys. Chem. Lett.* **2020**, *11*, 1840–1847.
- (88) Weigend, F.; Ahlrichs, R. Balanced Basis Sets of Split Valence, Triple Zeta Valence and Quadruple Zeta Valence Quality for H to Rn: Design and Assessment of Accuracy. *Phys. Chem. Chem. Phys.* **2005**, *7*, 3297.
- (89) Weigend, F. Accurate Coulomb-fitting Basis Sets for H to Rn. *Phys. Chem. Chem. Phys.* **2006**, *8*, 1057.

- (90) Ren, X.; Rinke, P.; Blum, V.; Wieferink, J.; Tkatchenko, A.; Sanfilippo, A.; Reuter, K.; Scheffler, M. Resolution-of-Identity Approach to Hartree–Fock, Hybrid Density Functionals, RPA, MP2 and GWwith Numeric Atom-Centered Orbital Basis Functions. *New J. Phys.* **2012**, *14*, 053020.
- (91) Eichkorn, K.; Treutler, O.; Öhm, H.; Häser, M.; Ahlrichs, R. Auxiliary Basis Sets to Approximate Coulomb Potentials. *Chem. Phys. Lett.* **1995**, 240, 283–290.
- (92) Weigend, F.; Köhn, A.; Hättig, C. Efficient Use of the Correlation Consistent Basis Sets in Resolution of the Identity MP2 Calculations. *J. Chem. Phys.* **2002**, *116*, 3175–3183.
- (93) Weigend, F.; Häser, M.; Patzelt, H.; Ahlrichs, R. RI-MP2: Optimized Auxiliary Basis Sets and Demonstration of Efficiency. *Chem. Phys. Lett.* **1998**, 294, 143–152.
- (94) Feller, D. The Role of Databases in Support of Computational Chemistry Calculations. *J. Comput. Chem.* **1996**, *17*, 1571–1586.
- (95) Schuchardt, K. L.; Didier, B. T.; Elsethagen, T.; Sun, L.; Gurumoorthi, V.; Chase, J.; Li, J.; Windus, T. L. Basis Set Exchange: A Community Database for Computational Sciences. *J. Chem. Inf. Model.* **2007**, 47, 1045–1052.
- (96) Pritchard, B. P.; Altarawy, D.; Didier, B.; Gibson, T. D.; Windus, T. L. New Basis Set Exchange: An Open, Up-to-Date Resource for the Molecular Sciences Community. *J. Chem. Inf. Model.* **2019**, *59*, 4814–4820.
- (97) Tschitschibabin, A. E. Über Einige Phenylierte Derivate Des p, p-Ditolyls. Ber. Dtsch. Chem. Ges. 1907, 40, 1810–1819.
- (98) Müller, E.; Pfanz, H. Über Biradikaloide Terphenylderivate. *Ber. Dtsch. Chem. Ges.* **1941**, *74*, 1051–1074.
- (99) Abe, M. Diradicals. Chem. Rev. 2013, 113, 7011-7088.
- (100) Duke Data Research Repository. http://doi.org/10.7924/r4wm1g15c. (Accessed 2023/05/01).

□ Recommended by ACS

Excited States, Symmetry Breaking, and Unphysical Solutions in State-Specific CASSCF Theory

Antoine Marie and Hugh G. A. Burton

MAY 04, 2023

THE JOURNAL OF PHYSICAL CHEMISTRY A

READ 🗹

Orthogonally Constrained Orbital Optimization: Assessing Changes of Optimal Orbitals for Orthogonal Multireference States

Saad Yalouz and Vincent Robert

FEBRUARY 15, 2023

JOURNAL OF CHEMICAL THEORY AND COMPUTATION

READ 🗹

R2022: A DFT/MRCI Ansatz with Improved Performance for Double Excitations

Dennis R. Dombrowski, Christel M. Marian, et al.

FEBRUARY 17, 2023

THE JOURNAL OF PHYSICAL CHEMISTRY A

READ [7

Fractional-Electron and Transition-Potential Methods for Core-to-Valence Excitation Energies Using Density Functional Theory

Subrata Jana and John M. Herbert

JUNE 13, 2023

JOURNAL OF CHEMICAL THEORY AND COMPUTATION

READ 🗹

Get More Suggestions >